

## Inertial mode interactions in a rotating tilted cylindrical annulus with free surface

Wenchao Xu \* and Uwe Harlander 

*Department of Aerodynamics and Fluid Mechanics,  
Brandenburg University of Technology (BTU) Cottbus – Senftenberg, 03046 Cottbus, Germany*



(Received 27 June 2019; accepted 28 August 2020; published 23 September 2020)

Rotating fluids frequently show nonlinear wave interactions and turbulence. This is true in particular for nonuniformly rotating systems. One example of such a nonuniform rotating object is the Earth. Due to its fast rotation it is not exactly spherical. As a result of the interaction with the Sun and Moon, the nonspherical Earth cannot rotate uniformly but shows precession and libration. This has consequences for the fluid enclosed in the outer Earth core. Due to the forcing it might become turbulent, one of the key factors in the present theories explaining the generation of the geomagnetic field. In the present paper we show experimental results from a system that is simpler than classical precession experiments but still shows very similar wave interactions and a collapse to turbulence. This system consists of a partly filled rotating annulus that rotates about its symmetry axis slightly tilted with respect to the gravity vector and allows us to explore Ekman numbers ranging from  $7.9 \times 10^{-6}$  to  $3.2 \times 10^{-5}$ . In analogy to the more classical precession experiments, we also find a resonant collapse when the forcing frequency corresponds with a resonant frequency of the rotating tank. The forced mode and two free Kelvin modes give rise to triadic resonance. Besides the parametric triadic resonance we further observed a shear-type instability of the nonlinearly excited geostrophic flow. This instability gives rise to a barotropic mode that interacts with the forced mode and generates secondary modes. We also observed a dependency of the mode frequencies on the Ekman number, which can, at least partly, be explained by a Doppler shift due to the mean flow. Finally, we try to connect our data to a low-order dynamical system that describes the main features of single triad interaction in precession experiments. Although this model is originally not designed for the multiple triads we observe, it is still useful for a qualitative understanding of mode interactions, e.g., for the mechanism of geostrophic mode excitation.

DOI: [10.1103/PhysRevFluids.5.094801](https://doi.org/10.1103/PhysRevFluids.5.094801)

### I. INTRODUCTION

The instabilities of the flow in a rotating container have been studied for a long time. Lord Kelvin (William Thomson) [1] linearized and solved the Euler equations, including rotation, by assuming time harmonic perturbations. This solution is composed by a sum of so-called normal Kelvin modes (i.e., inertial modes), where the Coriolis force plays the role of the restoring force. The frequency of each mode is less than two times the solid-body rotation frequency. These modes are damped when viscosity is added, unless external forcing provides the energy for their excitation.

Different experimental configurations have been used to excite Kelvin modes in a rotating container. McEwan [2] performed experiments with a slightly inclined top end in a fully filled axially rotating cylinder. Thompson [3] excited this periodic motion in a partly filled and slightly

---

\*wenchao.xu@b-tu.de

tilted rotating cylinder. Malkus [4], Malkus and Waleffe [5], and Le Bars *et al.* [6] used a rotating deformable elastic cylinder, which produces inertial modes with azimuthal wave number 2 or 3, depending on the deformation. Precession and libration are also common methods for exciting Kelvin modes. Experiments in a precessing cylinder were performed, e.g., by Manasseh [7], Meunier *et al.* [8], and Lagrange *et al.* [9,10], and in a longitudinal librating cylinder by Busse [11], Borcia *et al.* [12], and Klein *et al.* [13]. The container can also have different shapes, e.g., spherical, rather than cylindrical (Aldridge and Toomre [14], Hoff *et al.* [15,16]).

When the frequency of the excited Kelvin mode differs from the resonant frequency, the fluid response can be predicted by linear inviscid theory [17]. In contrast, when the forced Kelvin mode has the same frequency as one of the resonance frequencies of the rotating fluid, the Kelvin mode becomes unstable above a threshold amplitude. The instability leads to strong nonlinear effects and results in a sudden breakdown of the flow into small-scale disorder, which was referred to as “resonant collapse” by McEwan [2]. Later, in 1971 McEwan [18] suggested that the phenomenon can be explained with a triad resonance model, where two free modes form a triad in second-order resonant interaction with the forced mode. Exchanging energy with the forced mode, these free modes can lead to momentum mixing in localized regions, thus resulting in a breakdown of the inertial wave and eventually in the resonant collapse. The breakdown regimes at various Ekman numbers, precession angles, and frequencies have been studied and characterized by Manasseh [7]. At certain conditions, McEwan [18] and Manasseh [7] observed a relaminarization of the chaotic flow field after the breakdown and the rotating flow went into a breakdown-relaminarization cycle.

In a series of studies by Lopez and Marques [19–21], Meunier *et al.* [8–10] investigated triadic resonance in a precessing cylinder. Marques and Lopez [19] numerically studied the bifurcation of different states of triadic resonance under detailed parametric control and revealed the complex dynamics associated with weak precessional forcing. They [20] numerically investigated the influence of the nutation angle  $\alpha$  to the flow in a precessionally forced rotating cylinder, and their work reveals strong nonlinear and detuning effects depending on  $\alpha$ . With increasing  $\alpha$ , the system goes through different regimes, from a constant state to a tuned triadic resonance state, and subsequently follows a sequence of well-characterized bifurcations associated with triadic resonance. In their simulation, they observed that a mean flow (mode  $m = 0$ ) arises with increasing  $\alpha$ . Since the energy of the mean flow is provided by nonlinearity, a more inclined rotating cylinder with a stronger nonlinearity generates a stronger mean flow. We will see that the same is true for our setup. Meunier *et al.* [8] and Lagrange *et al.* [10] used linear stability theory to predict the spatial structure and the threshold for instability due to triadic resonance. They further developed a viscous and weakly nonlinear model to predict the resonant state and derive low-order amplitude equations by coupling the forced Kelvin mode with the two free modes and the geostrophic mode.

For the rotating cylinder with a nonzero background flow, a barotropic shear instability, similar to a parallel shear flow instability in a nonrotating system, might be induced, giving rise to an oscillating barotropic shear mode [22]. Thompson [3] has given the analytical prediction of the shear instability for a partly filled and slightly tilted rotating cylinder. Thompson further verified his theory experimentally and achieved good agreement. However, the velocity field was not analyzed qualitatively.

In the present research we experimentally study mode interactions in an inclined rotating annulus with a free surface. This is a setup of particular interest, since it is simpler than the precessing cylinder but in fact mimics aspects of rotating fluids forced by precession. This type of forcing is relevant for the dynamics of planetary bodies but also in the context of vortex dynamics: a rotating midlatitude low-pressure system is forced by precession too, since it rotates with the Earth [10]. The excitation and interaction of inertial waves in our study is similar to the partly filled rotating cylinder experiment by Thompson [3].

In our experiment we investigate the dominant features of the free surface configuration and compare them with the bounded precession counterpart. More generally, our study is also of interest in the context of the energy cascade in rotating fluids. The breakdown of the forced large scale mode transfers energy upscale to the balanced geostrophic mode but also downscale to other free

Kelvin modes. Such interactions are hence relevant for the still poorly understood energy transfer in geophysical flows.

Our research is also related to an engineering background. Instabilities could be induced due to the resonant effect in a spin-stabilized projectile with liquid payloads, which therefore could further disturb the flight stability. To avoid the resonance, a solution is to include a central rod in the cylindrical container and therefore to change the eigenfrequency. In this situation the model, as discussed in Selmi and Herbert [23], can be considered as a spinning and nutating cylindrical annulus, sharing similar features with our experimental configuration.

Finally, the study is also of interest in the context of unwanted Kelvin mode excitation [24], e.g., Rodda *et al.* [25] performed experiments with a differentially heated rotating annulus to study baroclinic waves. A global Kelvin mode was observed with a frequency equal to the annulus rotation, which was very likely driven by a slight inclination of the rotation axis.

The paper is structured in the following way: Section II describes the theoretical background and our experimental configuration. Section III introduces the wave breakdown in the tilted rotating cylindrical annulus with free surface. In Sec. IV we measure the geostrophic mode of the flow and compare the mean velocity profile in terms of the tilt angle. The influence of the tilt angle is then discussed. Section V discusses the secondary Kelvin modes and their interactions in the rotating flow. Different instabilities are responsible for the generation of the secondary modes. In Sec. VI we compare the experimental data with the results from a dynamical system of a classical precession experiment. Finally, conclusions are given in Sec. VII.

## II. EXPERIMENTAL BACKGROUND

In more classical precession experiments with circular cylinders with radius  $R$ , the cylinder is completely filled with fluid and rotates around its symmetry axis  $\hat{\mathbf{z}}$  with angular velocity  $\Omega$ . In addition, the cylinder rotates with  $\Omega_p$  around an axis that is inclined about an angle  $\alpha$  with respect to the cylinder's rotation axis. In this setup the direction of gravity does not play a role, and no other modes besides Kelvin modes can be excited. As is discussed in Zhang and Liao [26], for small Poincaré number  $0 < \text{Po} = \Omega_p/\Omega \ll 1$  and Ekman number  $\text{Ek} = \nu/(\Omega R^2) \ll 1$ , and further, a small amplitude of the fluid velocity in the cylinder,  $|\mathbf{u}| = \epsilon \ll 1$ , the nondimensional governing equations in the rotating frame of the cylinder (the mantle frame) read

$$\frac{\partial \mathbf{u}}{\partial t} + 2\hat{\mathbf{z}} \times \mathbf{u} + \nabla p = \text{Ek} \nabla^2 \mathbf{u} - 2\hat{\mathbf{z}} r \text{Po} \sin \alpha e^{i(t+\theta)}, \quad (1)$$

$$\nabla \cdot \mathbf{u} = 0. \quad (2)$$

The system is normalized by the cylinder radius  $R$  and the rotating rate  $\Omega$  in a cylindrical coordinate  $(\hat{\mathbf{r}}, \hat{\theta}, \hat{\mathbf{z}})$ . The equations need to be completed by nonslip boundary conditions. The last term in the first equation is the so-called Poincaré forcing that drives a Kelvin mode with azimuthal wave number  $m = 1$ .

In contrast to the precession system, the annulus in our experiment is not completely filled with fluid but has an upper free surface. It rotates around the symmetry axis  $\hat{\mathbf{z}}$  which is inclined by a small angle  $\alpha$  with respect to the direction of gravity. Obviously, in such a setup the Poincaré forcing term is missing; however, a Kelvin mode with  $m = 1$  is now driven by the upper boundary, see Fig. 1. The governing equation is

$$\frac{\partial \mathbf{u}}{\partial t} + 2\hat{\mathbf{z}} \times \mathbf{u} + \nabla p = \text{Ek} \nabla^2 \mathbf{u}, \quad (3)$$

$$\nabla \cdot \mathbf{u} = 0, \quad (4)$$

with the upper boundary condition for small angle  $\alpha$

$$w = dz/dt = \alpha r \cos(t + \theta). \quad (5)$$



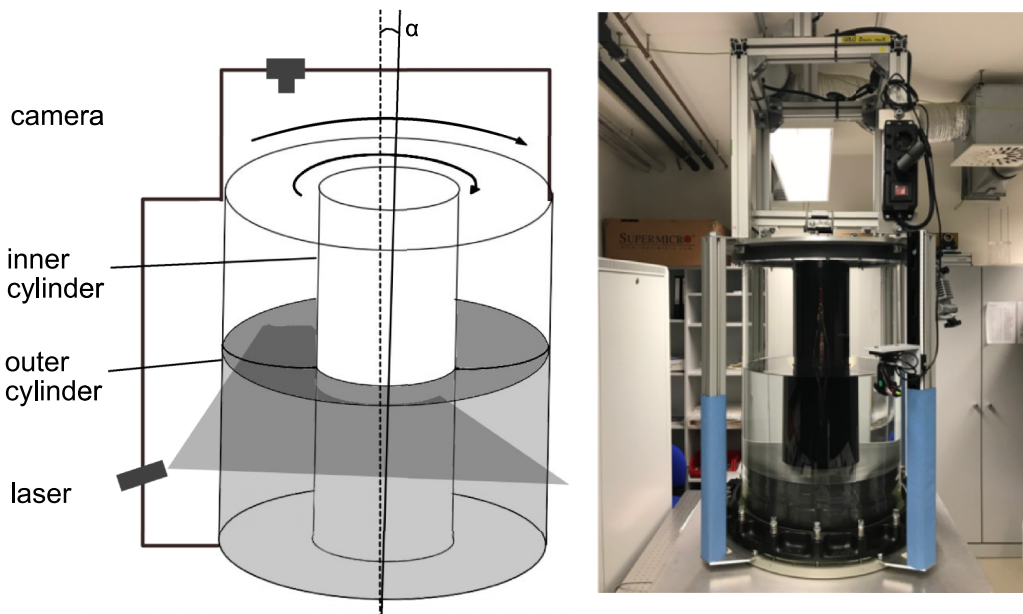


FIG. 2. (a) The schematic sketch and (b) photography of the laboratory apparatus.

Under certain circumstances the turbulent flow field can be relaminarized and enter a cycle of wave breaking and laminarization. The photographs in Fig. 3 show the phenomenon that we observed in the tilted rotating annulus; despite the fact that in our case we have a rotating annulus instead of a cylinder, the picture shows good agreement with the photography of the elliptically excited inertial wave taken by Malkus [28] and the photos of the classical precession experiment given in Manasseh [7].

As has been mentioned in the previous section, due to the existence of the free surface and the inclination of the annulus, the surface boundary condition is influenced by gravity; therefore a Kelvin mode is forced with azimuthal wave number  $m = 1$  and frequency  $\omega = 1$  when scaled by  $\Omega$ . At resonant frequency, a collapse of this forced mode happens following the sequence as shown in Fig. 3. In the photographs the left edge is the wall of the inner cylinder and the right is the outer cylinder. In Fig. 3(a) the fluid is in a stable state and the forced mode with the radial and axial wave number  $n = k = 1$  can easily be observed under illumination. The breakdown starts close to the inner cylinder, where a local disorder appears, see Fig. 3(b). This localized disorder moves with the crest of the forced mode and gradually expands to the whole annular gap within 20 revolutions. A further relaminarization can be observed, where the small-scale instabilities merge and the flow field becomes generally smoother compared with its most chaotic phase, as shown in Fig. 3(d).

The resonant frequency, i.e., the inertial mode eigenfrequency of the container, depends only on the container's geometry. An advantage of our free surface system is that we can easily control the aspect ratio through changing the water depth. Therefore the system can be well tuned to observe differences in the response of the fluid in the resonant or nonresonant regime.

The eigenfrequencies of inertial modes in a rotating annulus are derived in previous papers by Borcia and Harlander [29] and Lin *et al.* [30], where they solved (3) and (4) for small Ek with a solid wall boundary condition instead of the periodic upper boundary condition (5). The general solution is a sum of Kelvin modes of the spatial form

$$p(r, \theta, z) = p_{mnk}(r) \cos(k\pi z/h) e^{im\theta},$$

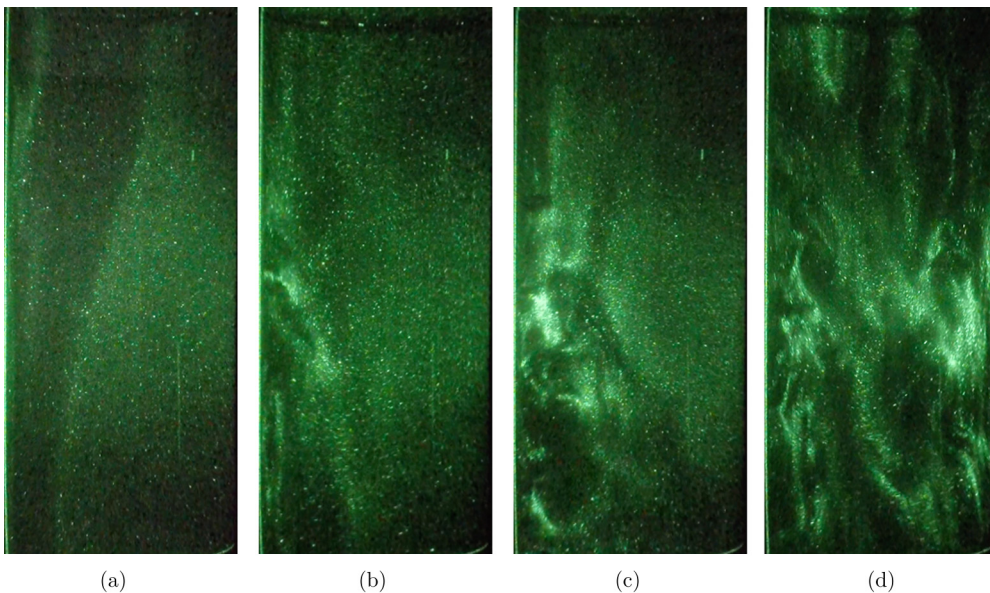


FIG. 3. Photographs of a vertical cross section of the annulus showing the process of the resonant collapse for  $Ek = 1.19 \times 10^{-5}$ ,  $Fr = 0.09$ , and water depth  $h = 1.2$ . The first photo (a) is taken at about 100 revolutions after starting rotation and the following photos are captured within 20 revolutions after (a). The left edge of the photograph represents the inner cylinder and the right edge the outer one.

$$\mathbf{u}(r, \theta, z) = \begin{pmatrix} u_{mnk}^r(r) \cos(k\pi z/h) \\ u_{mnk}^\theta(r) \cos(k\pi z/h) \\ u_{mnk}^z(r) \sin(k\pi z/h) \end{pmatrix} e^{im\theta}, \quad (6)$$

for the integral wave numbers  $m = 1, 2, 3, \dots$  and  $k = 1, 2, 3, \dots$ . The eigenfrequencies read

$$\omega^2 = \frac{4\pi^2}{(\xi h/k)^2 + \pi^2}, \quad (7)$$

and from the boundary conditions we find  $\xi$  from

$$r_i \xi^2 (P_{m+1} + P_{m-1}) - 2r_i \frac{\xi^2}{\omega} (P_{m+1} + P_{m-1}) + 2 \left( \frac{\xi h}{k\pi} \right)^2 m^2 P_m = 0, \quad (8)$$

where

$$P_m = J_m(\xi) Y_m(r_i \xi) - J_m(r_i \xi) Y_m(\xi). \quad (9)$$

Here  $r_i = R_i/R_o$  is the nondimensional radius of the inner cylinder and  $r_o = R_o/R_o = 1$  for the outer cylinder.  $J_m$  and  $Y_m$  are the first and second kind of Bessel functions for integer order  $m$ , and  $h$  is the water depth normalized as  $H/R_o$ . The mode frequency  $\omega_{mnk}^2 = \omega^2(\xi_{mnk})$ , where  $\xi_{mnk}$  is the  $n$ th positive solution of (8) for certain  $m$  and  $k$ . The integer  $n$  gives the number of nodes in the radial direction. Note that the structure of the solution in the radial direction, i.e.,  $p_{mnk}(r)$ ,  $u_{mnk}^r(r)$ ,  $u_{mnk}^\theta(r)$ ,  $u_{mnk}^z(r)$ , is also a sum of Bessel functions not given here.

Solving (7)–(9) for the forced Kelvin mode with wave number  $m = n = 1$  and forcing frequency  $\omega_f = 1$  gives  $h/k = 1.2$ . The frequencies of several Kelvin modes with  $m = 1$  and  $h = 1.2$  are listed in Table I. This result shows that the forcing frequency  $\omega_f = 1$  is very close to the frequency of the Kelvin mode  $\omega_{111} = 0.995$  when the water depth is  $h = 1.2$ , i.e., the forced Kelvin mode

TABLE I. The eigenfrequency of the inertial modes with azimuthal wave number  $m = 1$  for  $h = 1.2$ .

$n$	$k$	$\omega_{mnk}$	$\xi_{mnk}$	$n$	$k$	$\omega_{mnk}$	$\xi_{mnk}$
1	1	0.995	4.579	2	2	0.942	9.824
2	1	0.529	9.564	1	3	1.696	4.912
1	2	1.474	4.820	2	3	1.241	9.941

is very close to resonance for this water depth. The space-time diagram Fig. 4 measured by using Kalliroscope particles illuminated by a laser plane illustrates the temporal development of the forced Kelvin mode for different  $h$  ranging from 1.05 to 1.25. The wavy edge between the central bright zone and the dark zone on the left side indicates the amplitude of the forced Kelvin mode, which is most easily seen for  $h = 1.05$ . The period of the wavy shape is equal to one revolution of the cylinder. The amplitude of this wavy edge grows with increasing water depth. At  $h = 1.2$ , where the forced mode becomes resonant and matches with the eigenmode, the forced mode breaks down and leads to small-scale instabilities—a clear wavy edge can no longer be observed. With deeper water ( $h = 1.25$ ), the forced mode is away from resonance and the amplitude decreases. The wavy edge can then be identified again.

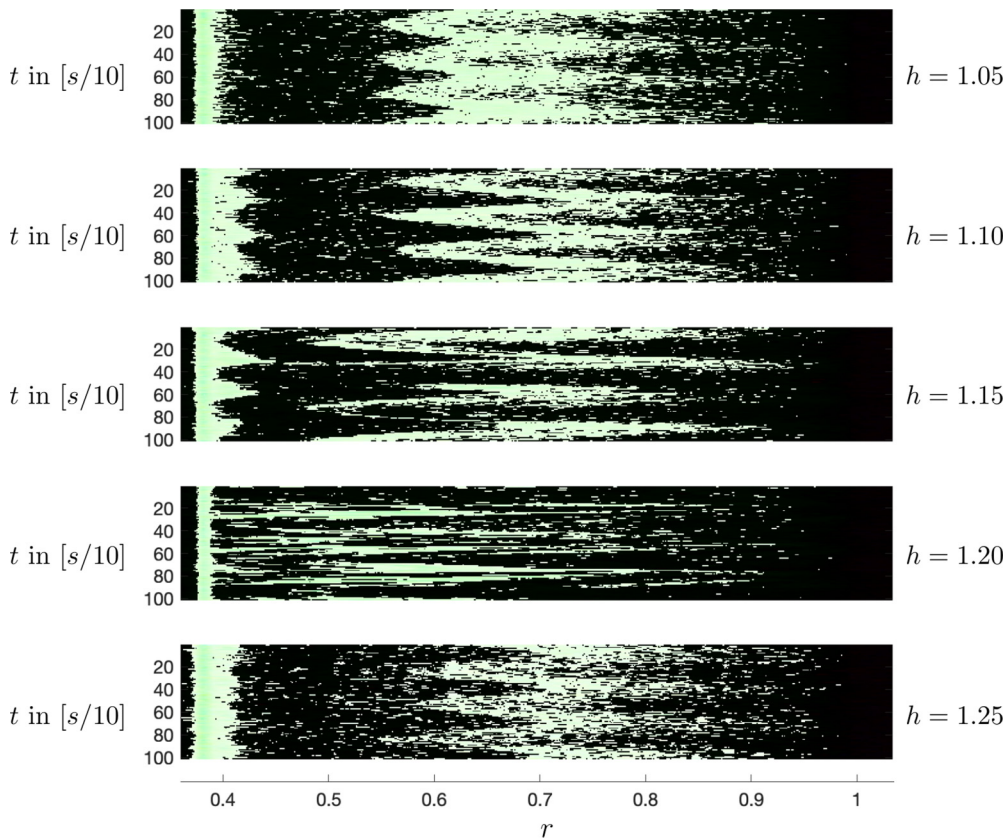


FIG. 4. Space-time diagrams for experiments with different  $h$  and for  $Ek = 1.19 \times 10^{-5}$ ,  $Fr = 0.09$  indicating the resonant collapse for  $h = 1.2$ .  $x$  axis: Radius, left represents inner cylinder and right outer cylinder;  $y$  axis: frame number (time in 0.1 s). The bright pixels are the laser reflected by the Kalliroscope seeded in the water.

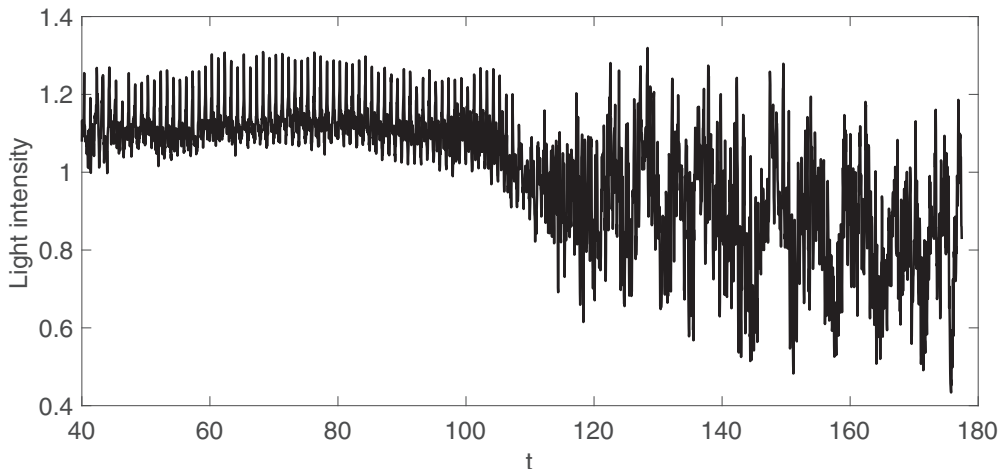


FIG. 5. Light intensity measured in the middle of the gap at  $z = 0.75h$  for  $Ek = 1.19 \times 10^{-5}$ ,  $Fr = 0.09$ , and  $h = 1.2$ . The distance between two sharp peaks equals one period of the rotation.

The resonant collapse can also be observed by measuring the light intensity of the fluid. Figure 5 shows the light intensity sampled at the center of the annulus gap as a function of time  $t$ . The time  $t$  is scaled by  $\Omega^{-1}$ , and  $t = 0$  denotes the start of the rotation. The absolute value of the light intensity has actually no clear physical meaning; however, violently fluctuating magnitude in a single video indicates strongly unstable flow. For  $t < 110$  the light intensity fluctuates at a regular frequency with a relative small amplitude; the flow is dominated by the forced Kelvin mode. The breakdown of the forced mode occurs at  $t \approx 110$ , after which the magnitude of the fluctuation grows significantly and the flow is obviously no longer dominated by a single mode. Nevertheless, the increased fluctuation of the light intensity indicates only a more unstable flow but not necessarily that the fluid velocity is increased. Fluid velocity measurement is presented in the following sections.

During the constant rotation of the fluid in an unstable state, a typical cycle of inertial wave breakdown and relaminarization has been observed. An unstable flow can become stable within a certain period after the breakdown, leading to a repetition of breakdown and relaminarization, as reported by McEwan [2], Thompson [3], and Manasseh [7]. Due to the limitation of the rotation rate of the current experimental facility, we are not able to prove whether for smaller  $Ek$  a sustained chaotic state exists, but in view of the similarity of our experiment with precessing cylinders it is likely.

#### IV. THE MEAN FLOW

To investigate whether the mean flow depends on the  $z$  axis, the mean azimuthal velocity  $u_\theta$  departure from the solid-body rotation is measured at different depth for  $\alpha = 1^\circ$  with a cover on the top of the annulus to avoid the wind during rotation, see Fig. 6. Each velocity profile is time-averaged over 200 revolutions and measured after a spin-up time much larger than the Ekman timescale. The gray color band is the standard deviation based on repeating the measurement at  $0.8h$  by completely restarting the experiment three times.

Apparently, the flow shows a negative velocity with a U-shape profile, which indicates that the fluid rotates slower than the tank. The maximum velocity magnitude is close to the inner cylinder. Note that due to the limitation of the PIV settings, the velocity in the boundary layer at the inner cylinder having a thickness of a few millimeters is unavailable. However, the turning point close to the inner cylinder (see black curve in Fig. 6) might be caused by the Ekman pumping in the boundary layer. In general, the velocity profiles at different depths show good agreement, with only small deviation with respect to  $z$ .

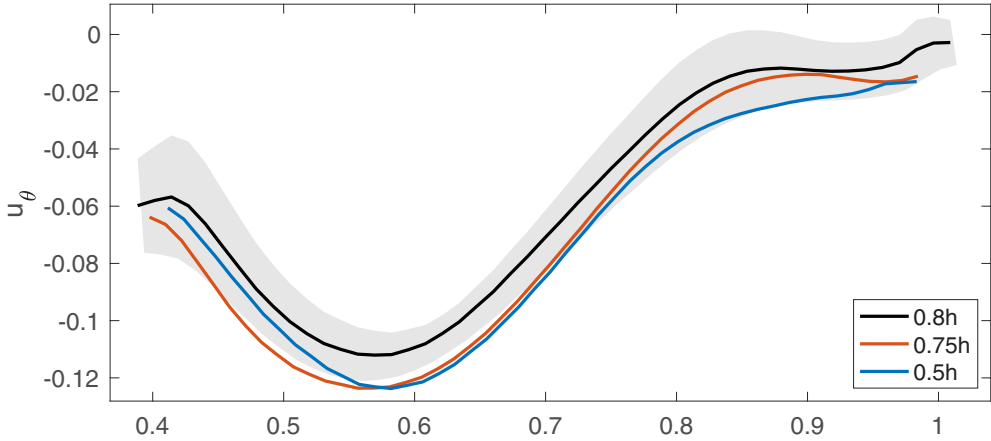


FIG. 6. Illustration of time-averaged nondimensional azimuthal velocity measured over 200 revolutions at different heights. The legend denotes the height of the laser plane from the bottom. Note that for  $0.8h$  we performed three measurements. The gray shading gives the standard deviation. The tank is tilted with angle  $\alpha \approx 1^\circ$ ,  $Ek = 1.19 \times 10^{-5}$ ,  $Fr = 0.09$ , and  $h = 1.2$ .

A common issue for the fluid in a rotating tank with a free surface is the wind effect. For an unclosed container, the air above the free surface does not corotate equally with the container. This velocity difference between air and water might slow down the surface water rotation and hence might influence the flow.

To verify the wind effect, experiments have been performed either with a lid at the top of the container or without any cover. The top lid forces the air in the gap to rotate uniformly with the container, thus eliminating the air drag on the water surface. Measurements are performed at the height  $0.88h$  that are close to the surface and the time-averaged azimuthal velocity profiles, shown in Fig. 7. The red dashed curve represents the profile with the cover on the top, while the black solid curve is without cover. Both experiments are measured with the same  $Ek$  at the same

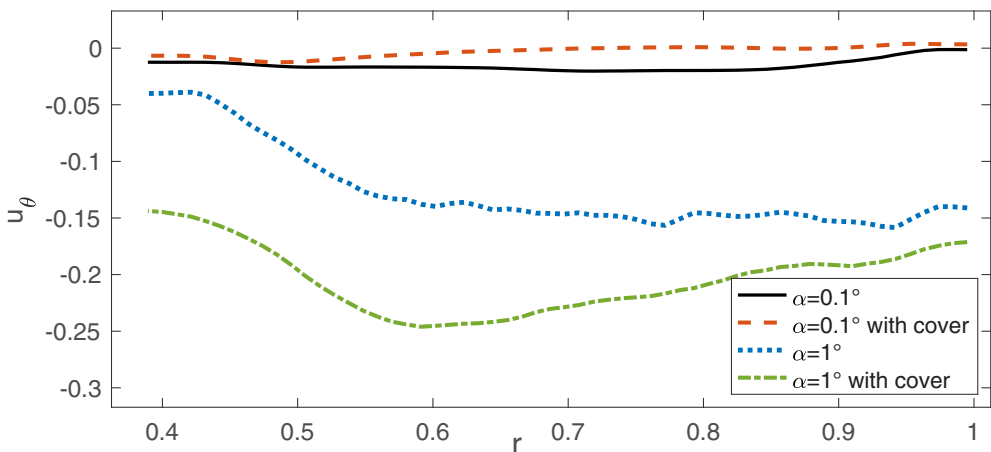


FIG. 7. Illustration of time-averaged nondimensional azimuthal velocity in radial direction measured at  $0.88h$ ; each data is averaged over 600 revolutions for  $Ek = 1.19 \times 10^{-5}$ ,  $Fr = 0.09$ , and  $h = 1.2$ . Black solid line: Tank without cover,  $\alpha \approx 0.1^\circ$ ; red dashed line: tank with top cover,  $\alpha \approx 0.1^\circ$ ; blue dot line: tank without cover,  $\alpha \approx 1^\circ$ ; green cross line: tank with top cover,  $\alpha \approx 1^\circ$ . (All other figures in the article are with top cover.)

position, and each case was repeated three times. Obviously, the fluid with the top cover has weaker retrograde flow, which proves that for the case with a small inclination angle  $\alpha$  the air torque is an important reason for the retrograde flow.

Nevertheless, the velocity close to the inner cylinder boundary still has an obvious deviation from zero, which implies another factor that influences the mean velocity profile. In fact, this profile is due to the nonlinear self-interaction of the forced mode mainly in the boundary layers.

With respect to a classical precession experiment, Kobine [31] states that the azimuthal flow results from the precessionally forced mode and an additional contribution related to nonlinear and viscous effects in the boundary layer. We think that for nonzero  $\alpha$  the mean flow is generated by a similar effect, except that the normal mode is forced by a gravitational torque on the nonaxisymmetric, viscously rotating mass instead of precessional forcing. It can be anticipated from (5) that the forced mode is stronger by increasing  $\alpha$ . Hence the nonlinear effect is more pronounced for an increased  $\alpha$ , which contributes to a stronger geostrophic mode.

To show this we performed further experiments by increasing  $\alpha$  from  $0.1^\circ$  to  $1^\circ$ , as shown in Fig. 7. The blue and green curves indicate the mean flow profile with increased  $\alpha$ . The significant difference between the experimental results for different tilt angles confirms our anticipation.

Nevertheless, referring to the mean flow profiles with  $\alpha \approx 1^\circ$ , the top cover also plays an important role, where the experiment without cover and hence with wind stress (blue curve in Fig. 7) surprisingly has a significantly weaker retrograde flow than that with cover (green curve in Fig. 7). A possible explanation is that the wind-induced Ekman layer damps the motions. In the previous section, the eigenfrequency of the cylindrical annulus was calculated from inviscid equations given in Lin *et al.* [30], where the Ekman pumping is not considered. This pumping, however, leads to an exponentially decreasing velocity profile in the boundary layer, thus influencing the effective aspect ratio for resonance [10,20]. The study of Borcia *et al.* [12] about the inertial mode in a rotating annulus with librating sidewall boundaries shows that the Stokes layer can influence the effective volume inside the container and therefore change the resonance frequency. Hence in our experiment the Ekman layer can also influence the effective volume and leads to a detuning of the resonant frequency and consequently, to a weaker forcing. Note that for a stronger mean flow, a barotropic shear instability can be induced [3]. This type of instability is discussed in the next section and in Sec. VII.

## V. KELVIN AND SHEAR MODES

The rotating flow of the tilted annulus can be regarded as a composition of a finite number of normal modes. The frequencies of the modes can easily be identified from the kinetic energy spectrum, as can be seen in Fig. 8. The figure shows the spectrum for  $\alpha \approx 0.1^\circ$  and  $1^\circ$  at the same rotation rate, where the kinetic energy is defined as  $E = \frac{1}{2}(u_\theta^2 + u_r^2)$ . Being mainly interested in the inertial modes, the range of the  $x$  axis is limited to  $0 \leq \omega \leq 2$ .

For  $\alpha \approx 0.1^\circ$  (the blue curve in Fig. 8), the flow is dominated by the forced mode with frequency  $\omega = 1$  together with a few secondary modes. Among the secondary modes, two modes with frequency 0.346 and 0.651 possess obviously more kinetic energy than the others. Note that the linear summation of the frequencies of these two modes equals the frequency of the forced mode, which suggests a possible triadic resonance. The peak at  $\omega = 0$  indicates the existence of a nonzero mean flow.

Increasing  $\alpha$  to  $1^\circ$ , the flow obviously becomes more energetic due to the forcing. The pattern of the modes is significantly changed with the appearance of more secondary modes. A prominent mode with frequency  $\omega = 0.195$  emerges which seems to be as strong as the forced mode. The frequencies of the modes still fulfill the triadic frequency condition.

The spatial structure of the Kelvin modes can be reconstructed by using harmonic analysis. To obtain a general view of the excited modes, the vorticity fields of the prominent modes are plotted in Fig. 9 for  $\text{Ek} = 1.19 \times 10^{-5}$  (20 rpm). Note that the figure is mainly for a qualitative understanding

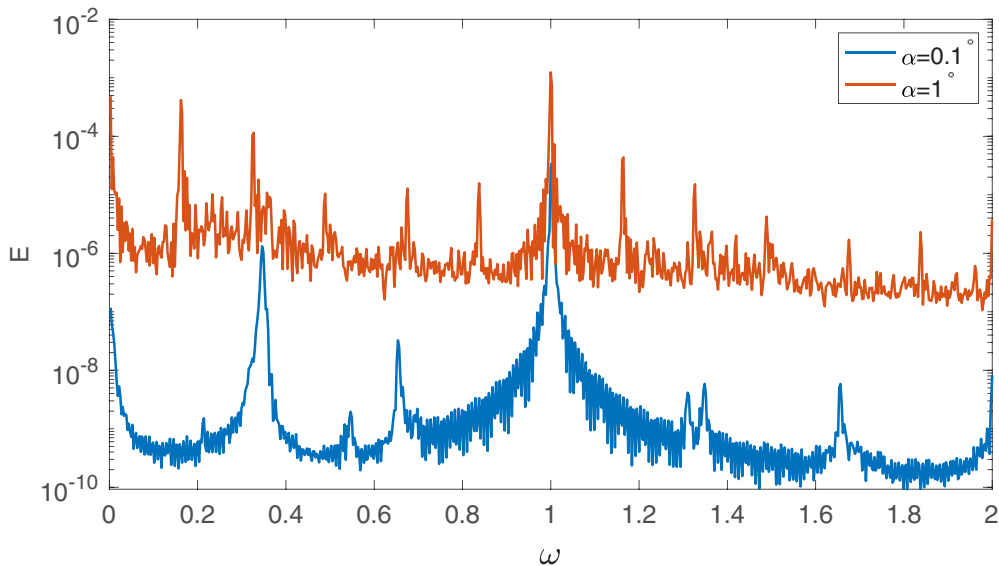


FIG. 8. Nondimensional kinetic energy spectrum  $E$  with different tilt angle  $\alpha$ .  $Ek = 1.19 \times 10^{-5}$ ,  $Fr = 0.09$ , and  $h = 1.2$ . Blue curve:  $\alpha = 0.1^\circ$ ,  $z = 0.75h$ ; red curve:  $\alpha = 1^\circ$ ,  $z = 0.8h$ .

of the mode structure; therefore a color bar is not provided and hence the same color for different modes does not imply the same vorticity magnitude.

The forced mode, which is excited due to the inclination of the cylinder [see (5)], rotates with the same angular velocity as the cylinder; therefore its normalized frequency  $\omega_1$  always equals 1, where the subscript of  $\omega$  denotes the azimuthal wave number of the respective mode. In fact, this resonant forced mode in the inclined rotating annulus has wave number 1 in azimuthal, axial, and radial direction. Its axial wave number can be acquired by seeding the fluid with Kalliroscope and inspecting the wave structure before the wave breakdown [see, e.g., Fig. 3(a)], and its azimuthal and radial wave number are acquired by using the harmonic analysis method [see Figs. 9(c) and 9(h)].

Figures 9(a) and 9(b) show the structure of the free Kelvin modes for  $\alpha \approx 0.1^\circ$ , which have azimuthal wave numbers  $m = 10$  and  $-9$ . The negative sign in front of the wave number indicates the wave propagates prograde and are hence faster than the annulus rotation, which is the opposite direction as the mean flow. Triadic resonance requires three modes in a triad to satisfy the parametric condition:  $\omega_i \pm \omega_{\mp j} = \omega_1$ ,  $m_i \pm m_{\mp j} = m_1$ , and  $k_i \pm k_{\mp j} = k_1$ , where the index 1 stands for the forced mode. The azimuthal wave number and the frequency of the two modes mentioned above satisfy these rules,  $m_{10} + m_{-9} = m_1$  and  $\omega_{10} + \omega_{-9} = \omega_1$ . Due to the strong mean flow in azimuthal direction, we cannot obtain accurate PIV data in a vertical section; therefore the axial wave number is generally not known from the horizontal PIV measurement.

### A. Mode interaction

To further verify the existence of triadic interactions, a bispectral analysis is applied by using the HOSA (high-order spectral analysis) MATLAB toolbox [15,32]. The bispectrum is defined as

$$B(\omega_x, \omega_y) = \frac{X(\omega_x)X(\omega_y)X^*(\omega_x + \omega_y)}{\sqrt{|X(\omega_x)|^2|X(\omega_y)|^2|X^*(\omega_x + \omega_y)|^2}}, \quad (10)$$

where  $X(\omega)$  is the Fourier transform and  $*$  denotes the complex conjugate. The sum of the bispectrum over a number of independent realizations, in our case, time series from different grid points, defines the bicoherence, which gives a statistical measure of quadratic phase coupling.

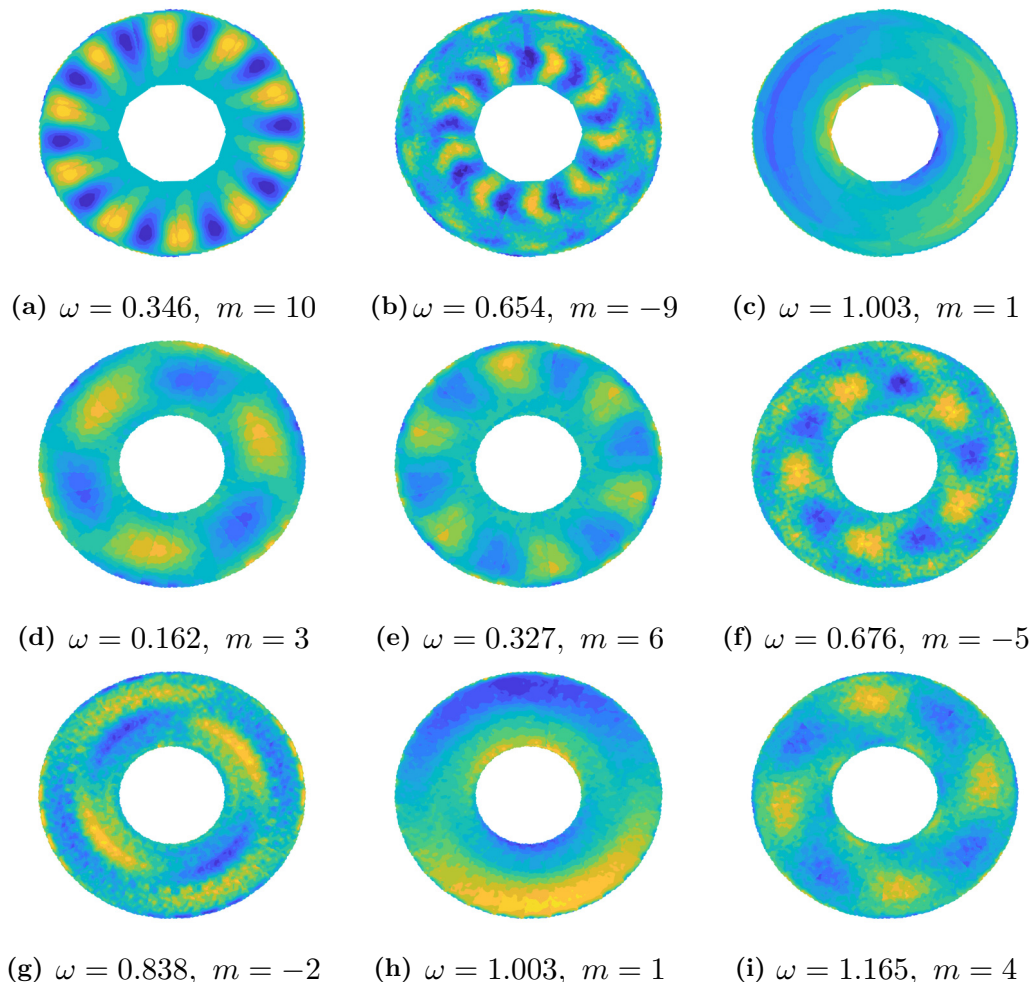


FIG. 9. Reconstruction of wave modes based on the velocity field for  $h = 1.2$ ,  $\text{Ek} = 1.19 \times 10^{-5}$ ,  $\text{Fr} = 0.09$ . The color represents the vorticity, where yellow (blue) indicates positive (negative) value of the vorticity. (a)–(c)  $\alpha \approx 0.1^\circ$ ,  $z = 0.75h$ ; (d)–(i)  $\alpha \approx 1^\circ$ ,  $z = 0.8h$ .

Figure 10(a) shows the bicoherence for  $\text{Ek} = 1.19 \times 10^{-5}$  and  $\alpha \approx 0.1^\circ$  of the azimuthal velocity component. Note that a bicoherence of 1 represents perfect triadic coupling of two modes and 0 means no coupling. The red spots in the diagram highlight the frequencies with strong bicoherence. The strong peaks on the line with  $\omega_x = \omega_y$  correspond to the self-correlation of the forced mode or the free modes. The diagram is symmetric with respect to the line  $\omega_x = \omega_y$ . The possible triads that resonate with the forced mode can be identified by connecting a line with slope  $-1$  between point  $(0, 1)$  and  $(1, 0)$ ; the points with high correlation on this line reveal the components of the triads as  $\omega_x$ ,  $\omega_y$  and  $\omega_x + \omega_y$  [33]. Thus the mode pair of frequency  $(0.346, 0.654)$  forms a triplet with the forced mode. The solutions of the dispersion relation (7) given in Table II suggest that the two modes are indeed free Kelvin modes with the wave numbers  $(10, 1, 1)$  and  $(-9, 2, 2)$ . The modes are generated due to a resonant breakdown of the forced Kelvin mode. However, the frequencies show no perfect match, indicating that the triad is not precisely tuned. Nevertheless, for  $\alpha \approx 0.1^\circ$  we found a scenario typical for triadic resonance.

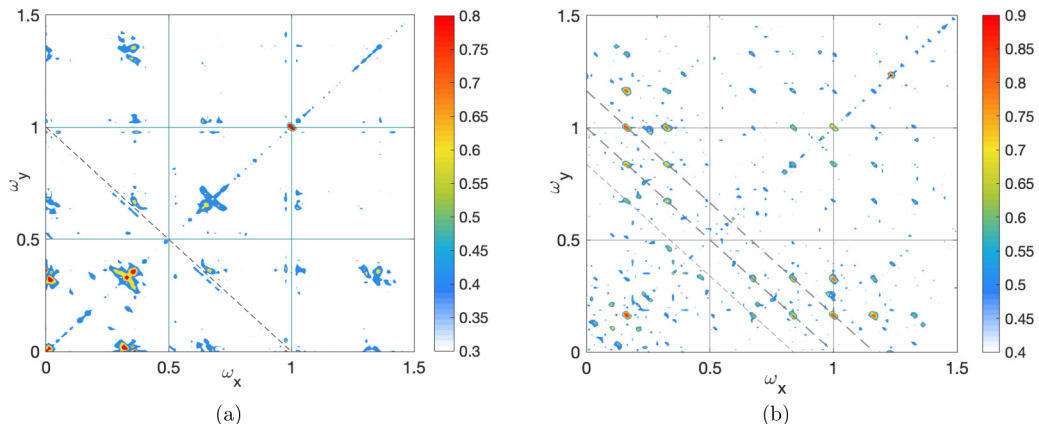


FIG. 10. Bicoherence spectrum for (a)  $\alpha \approx 0.1^\circ$  and (b)  $\alpha \approx 1^\circ$  with  $Ek = 1.19 \times 10^{-5}$ ,  $Fr = 0.09$ , and  $h = 1.2$ .

For  $\alpha \approx 1^\circ$ , the reconstructed most prominent modes are shown in Figs. 9(d)–9(i). Similar to  $\alpha \approx 0.1^\circ$ , the azimuthal wave numbers and the frequencies of the modes also satisfy the triadic resonance condition that  $m_3 + m_{-2} = m_6 + m_{-5} = m_4 - m_3 = m_1$  and  $\omega_3 + \omega_{-2} = \omega_6 + \omega_{-5} = \omega_4 - \omega_3 = \omega_1$ . Referring to the bicoherence spectrum [Fig. 10(b)], the mode pairs of frequency (0.838, 0.162) and (0.676, 0.327) form triplets with the forced mode. Furthermore, similar triplets can be found for the modes with frequency (0.838, 0.327) and (1, 0.162) with a mode of frequency  $\omega = 1.165$ , as well as the triplet (0.162, 0.676, 0.838). These multiple triplets indicate stronger nonlinear interactions between the modes for the case of stronger forcing.

However, the presence of a low-frequency  $m_3$  mode with  $\omega_3 = 0.162$  is surprising, since it seems that this mode is not a free Kelvin mode. A  $m_3$  Kelvin mode with small radial wave number has a much larger frequency, e.g., Kelvin eigenmodes with wave numbers (3,1,1) and (3,2,1) have frequencies of 0.799 and 0.485, respectively. This suggests that parametric triadic resonance is not the only instability in the flow for the case with strong forcing ( $\alpha \approx 1^\circ$ ).

A plausible explanation is that the low-frequency mode  $m_3$  is a low-frequency shear mode associated with barotropic shear instability. This instability is related to the presence of a nonzero geostrophic background flow in the rotating cylinder [3]. A similar instability has been reported by Herault *et al.* [34], where a low-frequency mode resulted from a destabilized azimuthal mean flow in a precessing cylinder. Herault *et al.* further related this instability to the theoretical prediction by Kerswell [28] that the dominant geostrophic shear mode interacts with the forced mode and gives rise to two subdominant Kelvin modes. The frequencies of the two subdominant Kelvin modes equal the linear combination of the forced mode and the geostrophic shear mode, which explains the triplets  $(m_1, m_3, m_{-2})$  and  $(m_1, m_3, m_4)$  in our experiments.

TABLE II. The eigenfrequency of the inertial modes with azimuthal wave number  $m = 10$  and  $-9$  for  $h = 1.2$ .

$m$	$n$	$k$	$\omega_{mnk}$	$\xi_{mnk}$	$m$	$n$	$k$	$\omega_{mnk}$	$\xi_{mnk}$
10	1	1	0.363	14.212	-9	1	2	0.707	13.867
10	2	1	0.285	18.200	-9	2	2	0.566	17.783
10	3	1	0.237	21.928	-9	3	2	0.473	21.553

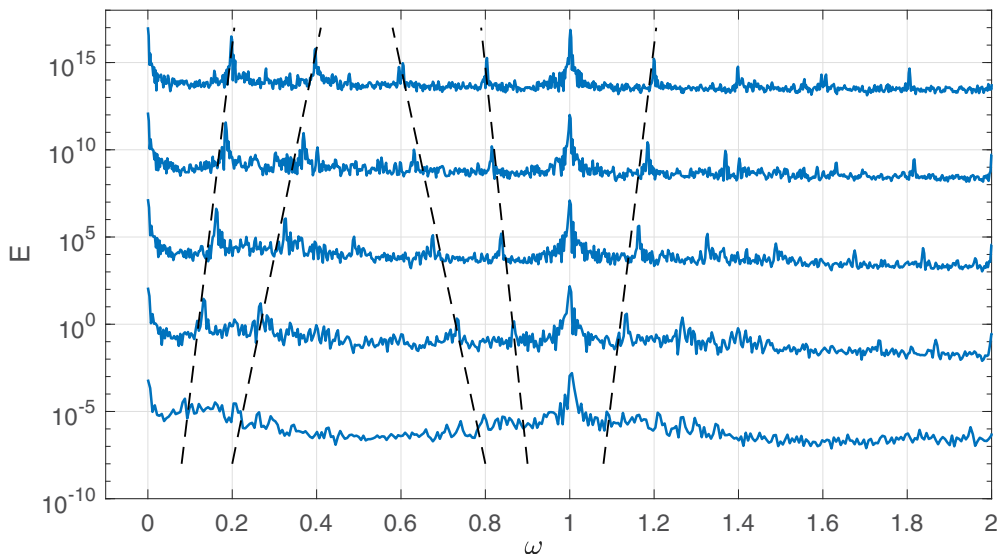


FIG. 11. Nondimensional kinetic energy spectrum at different angular velocities measured at  $0.8h$  with  $\alpha \approx 1^\circ$ . The curves in the diagram from bottom to top represent, respectively,  $Ek = 2.39 \times 10^{-5} - 1.59 \times 10^{-5} - 1.19 \times 10^{-5} - 9.55 \times 10^{-6} - 7.96 \times 10^{-6}$ . To separate the curves in y direction, a factor of  $10^5$  is multiplied for visualization. The black dashed line indicates the frequency variation of the respective mode with  $Ek$ .

The  $m_3$  mode might have a strong self-interaction, as can be seen from the red spot at  $(0.162, 0.162)$  in Fig. 10(b), which gives rise to the  $m_6$  mode. This  $m_6$  mode also interacts with the forced mode and results in the generation of the mode  $m_{-5}$  with its frequency  $\omega_{-5} = \omega_1 - \omega_6$ .

### B. Doppler shift

We noticed the dependency of the mode frequencies on the Ekman numbers for  $\alpha \approx 1^\circ$ . Figure 11 shows the variation of the mode frequency with  $Ek$  ranging from  $2.39 \times 10^{-5}$  to  $7.96 \times 10^{-6}$ . For the reader's convenience, we multiplied each two neighboring energy spectra by a factor of  $10^5$ . Obviously, we find similar peaks according to the energy spectra for the given  $Ek$ , and the harmonic analysis indicates that the wave numbers corresponding with the peaks are invariant of  $Ek$  for  $2.39 \times 10^{-5} \leq Ek \leq 7.96 \times 10^{-6}$ . On the other hand, the frequencies of the peaks vary with  $Ek$ . The frequency of the  $m_3$  mode constantly increases with the decrease of  $Ek$ , meanwhile the frequencies of the other modes change respectively so that the linear relation of the mode frequencies is robustly sustained during the considered range of  $Ek$ .

The frequencies of the free modes are plotted in Fig. 12(a) for a broader range of  $Ek$ . The frequency of mode  $m_3$  increases from a very low frequency (0.066) to 0.189 when  $Ek$  decreases from  $3.2 \times 10^{-5}$  to  $7.9 \times 10^{-6}$ , whereas mode  $m_2$ , which fulfils the relation  $\omega_3 + \omega_{-2} = \omega_1$ , shows a contrary tendency.

Since the camera system is fixed with the rotating frame, the influence of the Doppler effect on the measured frequency should be considered due to the presence of the mean flow in the azimuthal direction. An  $Ek$ -dependent frequency change was observed by Hoff *et al.* [15] when investigating inertial modes of spherical Couette flow. A frequency shift of the triad was discovered after transition from a weakly turbulent regime to a regular-inertial-mode regime. The authors attributed the frequency shift to the abrupt change of the mean flow through regime transition.

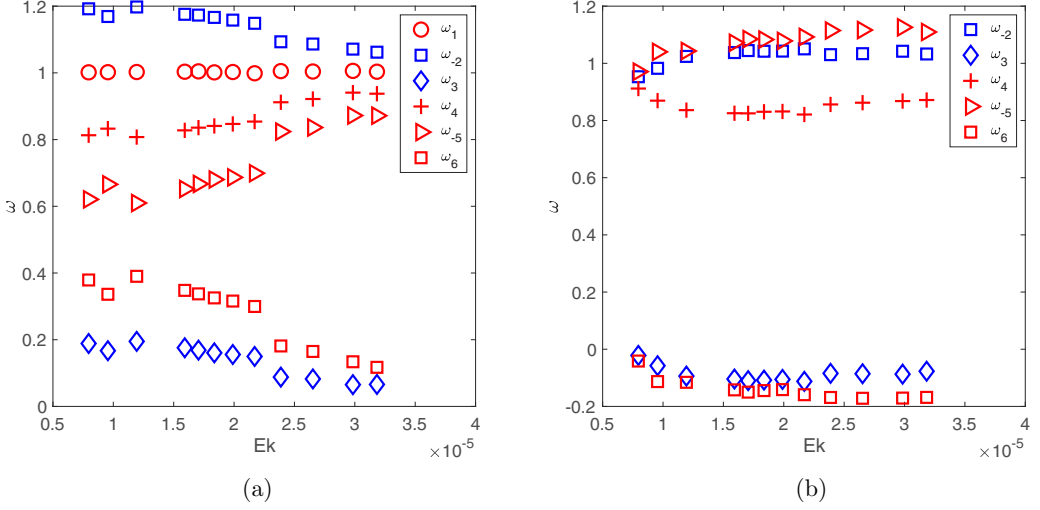


FIG. 12. Frequency distribution of the respective mode as a function of  $Ek$  at  $0.75h$  for  $h = 1.2$ : (a) measured frequency and (b) frequency corrected by the Doppler effect.

The shift of the frequency caused by the Doppler effect is estimated by

$$\Delta\omega = \Delta\Omega_\theta m = \frac{U_\theta}{R_o} m, \quad (11)$$

where  $\Delta\omega$  is the frequency change for different Ekman numbers,  $m$  is the nondimensional azimuthal wave number, and  $U_\theta$  is the mean azimuthal velocity in the rotating frame [15].

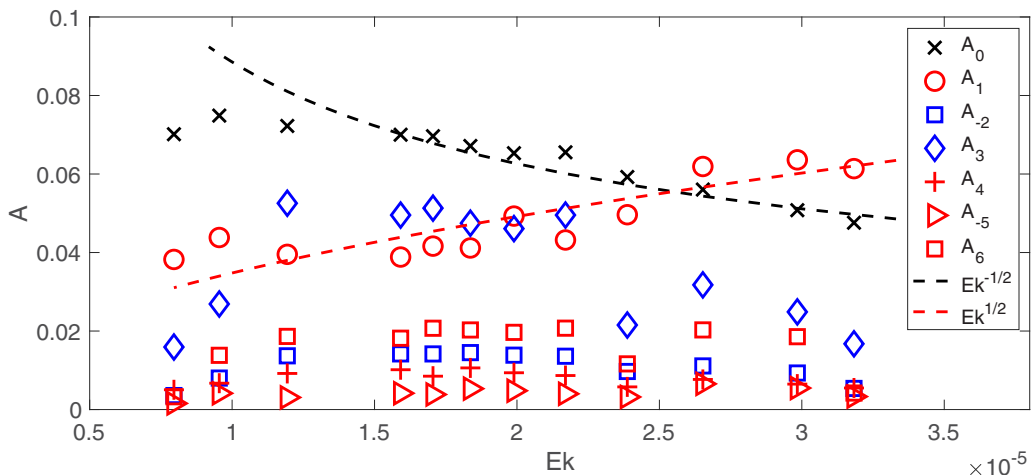
By considering the Doppler effect, the corrected intrinsic frequency as a function of  $Ek$  is plotted in Fig. 12(b). Generally speaking, the Doppler effect provides a reasonable correction to the frequency variation that reduces the change of the mode frequencies with regard to the Ekman numbers.

### C. Amplitudes

The amplitudes of the modes, defined as  $A_m = (u_{\theta,m}^2 + u_{r,m}^2)^{1/2}$ , are plotted as a function of  $Ek$  in Fig. 13 for  $7.79 \times 10^{-6} < Ek < 3.18 \times 10^{-5}$ . It must be noticed that the measured amplitude is not necessarily equal to the real amplitude of the mode due to the complex wave structure in the axial direction. However, assuming the axial structure of the respective mode keeps constant for different values of  $Ek$ , the relative size of the mode amplitude can be measured using data at a single depth.

For small  $Ek$ , the viscosity can be ignored in the interior of the rotating flow; however, this term has to be considered close to the boundary due to the presence of the Ekman layer. The nonlinear and viscous theory developed by Meunier *et al.* [8] shows that the mode amplitude is saturated by the viscous or the nonlinear effects or both. For high Ekman numbers, the mode amplitude is saturated by the viscous boundary layers and scales as  $Ek^{-1/2}$ . With the decrease of the Ekman number, the saturation due to the nonlinear effects becomes stronger and eventually dominant. Specifically, the nonlinear effects lead to the generation of the geostrophic mode, which in fact plays an important role in saturating the amplitude of the Kelvin modes. Actually, this mean-flow-related saturating effect is more significant than the saturation due to the nonlinear self-interaction of Kelvin modes.

In our experiment, the amplitude of the mean flow  $A_0$  (black crosses in Fig. 13) gets larger with decreasing  $Ek$ , whereas the forced mode  $A_1$  (red circles in Fig. 13) shows the opposite trend. The red and black dashed curves denote the scaling  $Ek^{1/2}$  and  $Ek^{-1/2}$ , respectively. The presence of the free Kelvin modes indicates that the rotating fluid is in a nonlinear regime. This implies a possibly


 FIG. 13. The mode amplitude as a function of  $Ek$  at  $0.75h$ ,  $h = 1.2$ .

weaker viscous saturation compared with the saturation due to the nonlinear effects. The change of  $A_0$  as a function of  $Ek$  suggests a strong dependency of the nonlinear effects on the Ekman number. For lower  $Ek$ , the nonlinear effects become stronger, promoting the generation of the mean flow and therefore increasing the saturation effect on the forced mode.

## VI. LOW-ORDER AMPLITUDE EQUATION

A weakly nonlinear model has been developed by Lagrange *et al.* [10] to describe the flow which couples the forced Kelvin mode to two free Kelvin modes and a geostrophic mode in a classical precessing cylinder. For the Ekman numbers of our experiment, this model shows irregular and possibly chaotic dynamics. However, we know that this is not the common route to turbulence for rotating fluids. On this route not a single triad becomes chaotic, but a cascading process leads to more and more triads and eventually to wave chaos [33]. From Fig. 10 we have learned that this process has started in our experiment. However, the single triad model by Lagrange *et al.* is still useful to understand certain aspects of the flow in our experiment.

In this weakly nonlinear model, the evolution of the geostrophic mode amplitude is given by

$$\frac{\partial A_0}{\partial t} = Ek^{1/2} \left( -\frac{2}{h} A_0 + \chi_2 |A_2|^2 + \chi_3 |A_3|^2 \right), \quad (12)$$

where  $A_0$ ,  $A_2$ , and  $A_3$  are, respectively, the amplitude of the geostrophic mode and two free Kelvin modes, and  $\chi_2$  and  $\chi_3$  are tuning constants. The first term on the right-hand side represents the viscous damping of the geostrophic mode, and the second and third terms represent the nonlinear self-interaction of the two free Kelvin modes driving the geostrophic mode. This equation suggests that the mean flow is generated due to the nonlinear self-interaction of the excited Kelvin modes and meanwhile damped by the viscous effects. Assuming  $\chi_2$  equals  $\chi_3$ , in a dynamical system with slow varying  $A_0$  ( $\frac{\partial A_0}{\partial t} / Ek^{1/2} \ll 1$ ),  $A_0 / (|A_2|^2 + |A_3|^2)$  should remain nearly constant so that  $(-\frac{2}{h} A_0 + \chi_2 |A_2|^2 + \chi_3 |A_3|^2)$  is close to 0.

Figure 14(a) shows the slow variation of the amplitudes of the geostrophic, the forced, and the free Kelvin modes for the experiment with  $Ek = 1.19 \times 10^{-5}$ . The amplitude time evolution is derived by applying a short-time Fourier transform over the velocity as follows:

$$A(t, \omega) = \left| \int_{-\infty}^{+\infty} u(\tau) h_w(\tau - t) e^{-i\omega\tau} d\tau \right| / \int_{-\infty}^{+\infty} h_w(\tau - t) d\tau, \quad (13)$$

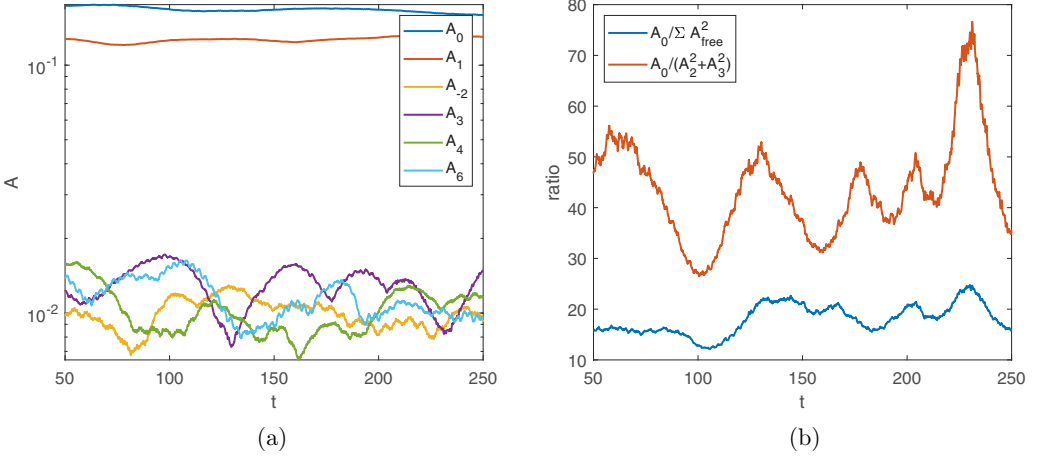


FIG. 14. (a) Amplitude of the modes and (b) ratios between  $A_0$  and nonlinear effects of different modes as a function of the dimensionless time  $t$ . Measured at  $0.8h$  with  $\text{Ek} = 1.19 \times 10^{-5}$ ,  $\text{Fr} = 0.09$ , and  $h = 1.2$ .

where  $h_w$  stands for the function of a smoothing Hamming window [33,35]. The geostrophic mode is plotted in blue in Fig. 14(a) and shows only a rather weak variation in time (i.e., a small standard deviation). In fact, the ratio between the data-based  $\frac{\partial A_0}{\partial t}$  and  $\text{Ek}^{1/2}$  is in the order of  $10^{-2}$ , i.e.,  $\frac{\partial A_0}{\partial t} \ll \text{Ek}^{1/2}$ .

For (12) this means that the ratio between  $A_0$  and  $|A_2|^2 + |A_3|^2$  should be close to a constant. It is obvious that for our experiment not only two free modes are excited. The Ek value in our case is more than one order of magnitude smaller, and the flow is closer to a turbulent state than that observed by Lagrange *et al.* [10]. However, their model, heuristically fitted to our case, is still useful in understanding some characteristics of the wave interactions. Hence we try to extend (12) by introducing the nonlinear self-interaction of all the free Kelvin modes. In this case, it is expected that  $A_0/\Sigma|A_{\text{free}}|^2$  remains nearly constant in time. Figure 14(b) shows the ratio between  $A_0$  and a number of squared amplitudes as a function of dimensionless time. It can be seen that, indeed,  $A_0/\Sigma|A_{\text{free}}|^2$  is nearly constant. In contrast, using just one triad leads to stronger variations (red curve).

Other information from (12) suggests that since  $h$  and  $\chi$  are independent of Ek, the ratio  $A_0/\Sigma|A_{\text{free}}|^2$  should also not depend on Ek. This ratio, taken from the experimental data as well as the numerical runs, is compared in Table III. The second row in the table is from the experimental measurements at  $0.8h$ , and the third row shows the numerical result from the model by Lagrange *et al.* [10] when all the parameters are kept fixed, but those given in the caption are adapted to our model. This means that we use  $h$  and Ek from our experiment. Note that the forcing in our experiment is larger, since in contrast to the precession experiment there is no small Poincaré

TABLE III. The ratio of  $A_0/\Sigma|A_{\text{free}}|^2$  for different Ek from experimental data measured at  $0.8h$  and  $A_0/\Sigma_{i=1}^2|A_{\text{free}}|^2$  from the model by Lagrange *et al.* [10] (at the fourth row) but for  $\text{Ro} = 30\text{Ro}_L = 30\Omega_p \sin \alpha / (\Omega + \Omega_p \cos \alpha)$ , where  $\Omega_p$  is the precession frequency,  $h = 1.2$ ,  $\chi = 0.003\chi_L$ , where the index  $L$  denotes the values used by Lagrange *et al.* [10].

Ek	$2.39 \times 10^{-5}$	$1.59 \times 10^{-5}$	$1.19 \times 10^{-5}$	$9.55 \times 10^{-6}$	$7.96 \times 10^{-6}$
$A_0/\Sigma A_{\text{free}} ^2$	33.82	24.28	28.02	24.98	21.25
$A_0/\Sigma_{i=1}^2 A_{\text{free}} ^2$	18.18	18.03	18.25	17.85	17.50

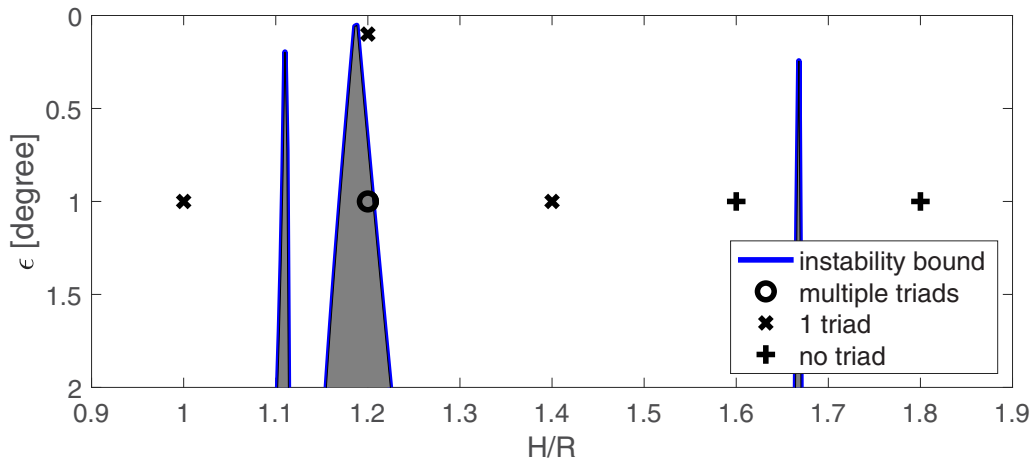


FIG. 15. Theoretical prediction of the shear instability in the annulus for  $Ek = 1.19 \times 10^{-5}$  and  $Fr = 0.09$ . The symbols show whether mode triads exist for  $0 < \omega \leq 1$  from experimental results. The figure should be compared with Fig. 4 by Thompson [3].

number in the forcing term [see (3) and (5)]. We used a value for  $Ro$  that is 30 times larger than that used by Lagrange *et al.* The tuning parameter  $\chi$  was adapted in the following way: from Fig. 14(b) we read off the constant for  $A_0/\Sigma|A_{free}|^2$ . Then we determined  $\chi$  by  $\chi = \frac{2}{\bar{r}}A_0/\Sigma|A_{free}|^2$ , which gives a  $\chi$  value that is a factor  $3 \times 10^{-3}$  smaller than the value used by Lagrange *et al.* [10].

Note again that the experimental measurements give the amplitude of the modes at a certain depth which might not necessarily be equal to the mode amplitude when we would have access to the full axial structure of the mode. However, we compare the dependency of  $A_0/\Sigma|A_{free}|^2$  with respect only to  $Ek$ , and the magnitude of this ratio is not relevant here.

Although, as discussed in the previous section, we find a disagreement between our free surface and the classical precessing experiment, namely, that the strength of the nonlinear effects is influenced by  $Ek$  in our case, the experimental results reveal that  $A_0/\Sigma|A_{free}|^2$  depends only very weakly on the Ekman numbers, which is consistent with the weakly nonlinear model designed for the precessing cylinder [10]. Therefore this analysis confirms that for the tilted rotating annulus with free surface, the nonlinear self-interaction of the free Kelvin modes becomes stronger for decreasing  $Ek$  and implies an increase of mean flow amplitude such that the ratio  $A_0/\Sigma|A_{free}|^2$  remains constant.

## VII. DISCUSSION AND CONCLUSION

A series of experiments have been performed to investigate the mode interaction in a tilted rotating annulus with free surface. In the experiments, two modes play a major role for the dynamics: a forced Kelvin mode, which is driven by the gravitational torque on the nonaxisymmetric viscously rotating mass, and a geostrophic mode, i.e., a mean flow, generated by nonlinear wave-wave interactions. Free Kelvin modes and shear modes are given rise by instabilities of the forced mode and the geostrophic mode, respectively.

Due to the inclination of the annulus, a forced Kelvin mode with wave number  $m = n = k = 1$  and frequency  $\omega = 1$  is excited. The amplitude of the forced Kelvin mode grows rapidly when the mode is close to an eigenmode of the annulus. Once the amplitude of the forced mode exceeds a threshold value, the mode becomes oversaturated, breaks down, and leads to a resonant collapse as described for the precessing cylinder experiment by McEwan [2] and Manasseh [7]. Two well-tuned subdominant free Kelvin modes are excited during this process and form a triad with the forced Kelvin mode. This corresponds to a typical scenario of the triadic resonance.

Besides the parametric triadic instability, we also observed a shear-type instability that is related to the nonzero mean flow, i.e., the geostrophic mode. The experimental result confirms that similar to the precessing cylinder experiment carried out by Kobine [31], the mean flow increases with the tilt angle  $\alpha$  [see (5)]. For a sufficiently strong mean flow, a shear-type instability is excited and gives rise to a low-frequency barotropic shear mode. This shear mode interacts with the forced Kelvin mode and generates two free Kelvin modes that satisfy the triadic relation with the shear mode and the forced mode.

Shear instabilities in a partially filled and tilted rotating full cylinder have been studied by Thompson [3], who presented a theoretical prediction of the instability bounds. Following Thompson, we predicted the bounds of the shear instability for our experiment with annular geometry and experimentally verified the existence of the shear instability for different aspect ratios (fluid depths). The result is shown in Fig. 15, where the shaded areas represent shear instabilities. The symbols show the number of triads we find experimentally in the frequency range  $0 < \omega \leq 1$ . In this range the most prominent triads can be found.

The open circle indicates that more than one triad emerges, where the shear instability not only induced a low-frequency mode  $m_3$  but also its harmonic mode  $m_6$ , as discussed in Sec. V. Both modes interact with the forced Kelvin mode and give rise to additional free Kelvin modes. The shear instability necessitates a sufficiently strong mean flow, which requires a large forcing, e.g., large inclination angle of the annulus. A resonant fluid depth helps to strengthen the mean flow by a coupling to free modes. On the other hand, when the forcing is weak ( $\alpha = 0.1^\circ$ ) and hence the nonlinearly driven shear flow is too weak for becoming unstable, the forced Kelvin mode can still become unstable due to resonance, e.g., when  $H/R$  is close to 1.2 (see cross above  $H/R = 1.2$  in Fig. 15). As shown by crosses in Fig. 15, if  $H/R$  is close enough to the resonance depth (e.g., for  $H/R = 1$  or  $H/R = 1.4$ ), a triadic resonant instability occurs and induces two free Kelvin modes satisfying the triadic relation with the forced Kelvin mode. Finally, if we are outside the depths for shear instability and too far away from the resonant depth, only the forced mode can be observed.

We observed that the Ekman number has a prominent impact on the frequencies of the excited modes, except the frequency of the forced Kelvin mode. The frequencies of the retrograde modes increase with decreasing  $Ek$ , whereas the frequencies of the prograde modes have an opposite trend. The Doppler shift due to the strong background flow is found to be mainly responsible for this behavior. A recent paper by Haurault *et al.* [34] also points out that the nonzero background flow modifies the dispersion relation and thus detunes the frequency of Kelvin modes.

In fact, our experiment exhibits some similar characteristics when compared to the precessing cylinder experiment by Haurault *et al.* [34], where they reported the presence of the parametric triadic resonance as well as a low-frequency barotropic mode interacting with the forced Kelvin mode. A similar quasigeostrophic  $m_3$  mode has also been observed in late stages of the so-called conical shear instability. As reported by Lin *et al.* [36], this instability occurred after a parametric triadic instability inside a precessing sphere. Although the geometry differs from the cylindrical case, the excited modes show many similarities.

Moreover, in our experiment with a free surface, a higher harmonics of the barotropic shear mode has been noticed that is also part of the triads with the forced mode. The bicoherence spectrum further confirms triadic interactions between the modes and reveals also triads between three free Kelvin modes for the multiple triad case. We also attempt to connect the low-order dynamical system by Lagrange *et al.* [10] to our data. Although in our case more modes are active than contained in the low-order model, we could confirm that the geostrophic mode is balanced by a forcing due to self-interacting free modes and viscous damping. In future work we will try to better adapt the dynamical system to our experiment so that we could have a simple tool for understanding the nonlinear interactions between the excited modes and to find thresholds for regime transitions.

Aside from the common phenomena that have been observed in classical precessing experiments, we also observed some remarkable characteristics that deviate from what has been found in the precession setups. For example, in our experiment the amplitudes of the forced Kelvin mode and the geostrophic mode are saturated mainly due to the nonlinear effects. For the classical precession

setup, theoretical and experimental results show that nonlinear effects are independent of the Ekman numbers. However, our experiment shows that the nonlinear effects significantly depend on  $Ek$ , which seems to scale roughly with  $Ek^{-1/2}$  (see red dashed curve in Fig. 13). The nonlinear dependency further influences the amplitude of the mean flow and the saturation of the forced Kelvin mode.

Presently, our experiments are conducted within a relative narrow range of Ekman numbers and a fixed inclination angle, which leaves plenty of space for further explorations. The existence of a free surface introduces extra complexity into the rotating system. Nevertheless, it is useful for further study, since it provides a convenient approach to investigate wave interactions and the influence of the aspect ratio on resonance. As suggested by Meunier [37], the open surface rotating cylinder might also be important for technical applications. This system might improve bioreactors, since mixing due to the resonant collapse is much less destructive than mixing with rotating blades.

### ACKNOWLEDGMENTS

The work is part of the cluster “Stochastic Methods for Fluid Flow and Transport Processes” in the frame of the Graduate Research School (GRS) of Brandenburg University of Technology Cottbus-Senftenberg, and we thank BTU for financial support. W.X. and U.H. acknowledge the financial support from DFG Grant No. HA 2932/8-2. The authors would like to thank Patrice Meunier and Patrice Le Gal (IRPHE, CNRS, Aix Marseille University) for fruitful scientific discussions, and Ludwig Stapelfeld, Robin Stöbel, Vilko Ruoff, and Heinz-Jörg Wengler for technical support. Finally, we thank two anonymous reviewers for their suggestions that improved the clarity of the paper. In particular, we are grateful to one of the reviewers for suggesting that we consider the possibility of shear instability and earlier work on this topic.

- 
- [1] W. Thomson, XXIV. Vibrations of a columnar vortex, *London, Edinburgh, Dublin Philos. Mag. J. Sci.* **10**, 155 (1880).
  - [2] A. D. McEwan, Inertial oscillations in a rotating fluid cylinder, *J. Fluid Mech.* **40**, 603 (1970).
  - [3] R. Thompson, Diurnal tides and shear instabilities in a rotating cylinder, *J. Fluid Mech.* **40**, 737 (1970).
  - [4] W. V. R. Malkus, An experimental study of global instabilities due to the tidal (elliptical) distortion of a rotating elastic cylinder, *Geophys. Astrophys. Fluid Dyn.* **48**, 123 (1989).
  - [5] W. V. R. Malkus and F. A. Waleffe, Transition from order to disorder in elliptical flow: A direct path to shear flow turbulence, in *Advances in Turbulence 3*, edited by A. V. Johansson and P. H. Alfredsson (Springer, Berlin, 1991), pp. 197–203.
  - [6] M. Le Bars, S. Le Dizès, and P. Le Gal, Coriolis effects on the elliptical instability in cylindrical and spherical rotating containers, *J. Fluid Mech.* **585**, 323 (2007).
  - [7] R. Manasseh, Breakdown regimes of inertia waves in a precessing cylinder, *J. Fluid Mech.* **243**, 261 (1992).
  - [8] P. Meunier, C. Eloy, R. Lagrange, and F. Nadal, A rotating fluid cylinder subject to weak precession, *J. Fluid Mech.* **599**, 405 (2008).
  - [9] R. Lagrange, C. Eloy, F. Nadal, and P. Meunier, Instability of a fluid inside a precessing cylinder, *Phys. Fluids* **20**, 081701 (2008).
  - [10] R. Lagrange, P. Meunier, F. Nadal, and C. Eloy, Precessional instability of a fluid cylinder, *J. Fluid Mech.* **666**, 104 (2011).
  - [11] F. H. Busse, Zonal flow induced by longitudinal librations of a rotating cylindrical cavity, *Physica D* **240**, 208 (2011).
  - [12] I. D. Borcia, G. V. Abouzar, and U. Harlander, Inertial wave mode excitation in a rotating annulus with partially librating boundaries, *Fluid Dyn. Res.* **46**, 041423 (2014).

- [13] M. Klein, T. Seelig, M. V. Kurgansky, A. Ghasemi V, I. D. Borcia, A. Will, E. Schaller, C. Egbers, and U. Harlander, Inertial wave excitation and focusing in a liquid bounded by a frustum and a cylinder, *J. Fluid Mech.* **751**, 255 (2014).
- [14] K. D. Aldridge and A. Toomre, Axisymmetric inertial oscillations of a fluid in a rotating spherical container, *J. Fluid Mech.* **37**, 307 (1969).
- [15] M. Hoff, U. Harlander, and S. A. Triana, Study of turbulence and interacting inertial modes in a differentially rotating spherical shell experiment, *Phys. Rev. Fluids* **1**, 043701 (2016).
- [16] M. Hoff, U. Harlander, and C. Egbers, Experimental survey of linear and nonlinear inertial waves and wave instabilities in a spherical shell, *J. Fluid Mech.* **789**, 589 (2016).
- [17] H. P. Greenspan, *The Theory of Rotating Fluids* (Cambridge University Press, Cambridge, UK, 1968).
- [18] A. D. McEwan, Degeneration of resonantly-excited standing internal gravity waves, *J. Fluid Mech.* **50**, 431 (1971).
- [19] F. Marques and J. M. Lopez, Precession of a rapidly rotating cylinder flow: Traverse through resonance, *J. Fluid Mech.* **782**, 63 (2015).
- [20] J. M. Lopez and F. Marques, Nonlinear and detuning effects of the nutation angle in precessionally forced rotating cylinder flow, *Phys. Rev. Fluids* **1**, 023602 (2016).
- [21] J. M. Lopez and F. Marques, Rapidly rotating precessing cylinder flows: Forced triadic resonances, *J. Fluid Mech.* **839**, 239 (2018).
- [22] F. H. Busse, Shear flow instabilities in rotating systems, *J. Fluid Mech.* **33**, 577 (1968).
- [23] M. Selmi and T. Herbert, Resonance phenomena in viscous fluids inside partially filled spinning and nutating cylinders, *Phys. Fluids* **7**, 108 (1995).
- [24] J. Boisson, D. Cébron, F. Moisy, and P. P. Cortet, Earth rotation prevents exact solid-body rotation of fluids in the laboratory, *Europhys. Lett.* **98**, 59002 (2012).
- [25] C. Rodda, I. D. Borcia, P. Le Gal, M. Vincze, and U. Harlander, Baroclinic, Kelvin and inertia-gravity waves in the barostrat instability experiment, *Geophys. Astrophys. Fluid Dyn.* **112**, 175 (2018).
- [26] K. Zhang and X. Liao, *Theory and Modeling of Rotating Fluids, Convection, Inertial Waves and Precession*, Cambridge Monographs on Mechanics (Cambridge University Press, Cambridge, 2017).
- [27] T. Albrecht, H. M. Blackburn, J. M. Lopez, R. Manasseh, and P. Meunier, Triadic resonances in precessing rapidly rotating cylinder flows, *J. Fluid Mech.* **778**, 62 (2015).
- [28] R. R. Kerswell, Secondary instabilities in rapidly rotating fluids: Inertial wave breakdown, *J. Fluid Mech.* **382**, 283 (1999).
- [29] I. D. Borcia and U. Harlander, Inertial waves in a rotating annulus with inclined inner cylinder: Comparing the spectrum of wave attractor frequency bands and the eigenspectrum in the limit of zero inclination, *Theor. Comput. Fluid Dyn.* **27**, 397 (2012).
- [30] Y. Lin, J. Noir, and A. Jackson, Experimental study of fluid flows in a precessing cylindrical annulus, *Phys. Fluids* **26**, 046604 (2014).
- [31] J. J. Kobine, Azimuthal flow associated with inertial wave resonance in a precessing cylinder, *J. Fluid Mech.* **319**, 387 (1996).
- [32] C. L. Nikias and M. R. Raghuveer, Bispectrum estimation – A digital signal-processing framework, *Proc. IEEE* **75**, 869 (1987).
- [33] C. Brouzet, E. V. Ermanyuk, S. Joubaud, I. Sibgatullin, and T. Dauxois, Energy cascade in internal-wave attractors, *Europhys. Lett.* **113**, 44001 (2016).
- [34] J. Hérault, A. Giesecke, T. Gundrum, and F. Stefani, Instability of precession driven Kelvin modes: Evidence of a detuning effect, *Phys. Rev. Fluids* **4**, 033901 (2019).
- [35] F. Auger, P. Flandrin, P. Gonçalvès, and O. Lemoine, Time-frequency toolbox, CNRS France-Rice University (1996), <http://nongnu.org/tftb/tutorial.pdf>.
- [36] Y. Lin, P. Marti, and J. Noir, Shear-driven parametric instability in a precessing sphere, *Phys. Fluids* **27**, 046601 (2015).
- [37] P. Meunier, Soft mixer: Toward geoinspired bioreactors, *J. Fluid Mech.* (to be published).